SPECTROSCOPIC STUDIES OF THE SOLAR CORONA

V. *Physical Properties of Coronal Structures*

JAGDEV SINGH[1], TAKASHI SAKURAI[2], KIYOSHI ICHIMOTO[2] and S. MUNEER[3]
[1]*Indian Institute of Astrophysics, Bangalore 560034, India (e-mail: jsingh@iiap.ernet.in)*
[2]*National Astronomical Observatory, 2-21-1, Ohsawa, Mitaka, Tokyo, 181-85 88, Japan*
[3]*Indian Institute of Astrophysics, Kodaikanal – 624103, India (e-mail: muni@iiap.ernet.in)*

(Received 2 July 2002; accepted 9 October 2002)

Abstract. Spectra around the 6374 Å [Fe X] and 7892 Å [Fe XI] emission lines were obtained simultaneously with the 25-cm coronagraph at Norikura Observatory covering an area of $200'' \times 500''$ of the solar corona. The line width, peak intensity and line-of-sight velocity for both the lines were computed using Gaussian fits to the observed line profiles at each location ($4'' \times 4''$) of the observed coronal region. The line-width measurements show that in steady coronal structures the FWHM of the 6374 Å emission line increases with height above the limb with an average value of 1.02 mÅ arc $\sec^{-1}$. The FWHM of the 7892 Å line also increases with height but at a smaller average value of 0.55 mÅ arc $\sec^{-1}$. These observations agree well with our earlier results obtained from observations of the red, green, and infrared emission lines that variation of the FWHM of the coronal emission lines with height in steady coronal structures depends on plasma temperatures they represent. The FWHM gradient is negative for high-temperature emission lines, positive for relatively low-temperature lines and smaller for emission lines in the intermediate temperature range. Such a behaviour in the variation of the FWHM of coronal emission lines with height above the limb suggests that it may not always be possible to interpret an increase in the FWHM of emission line with height as an increase in the nonthermal velocity, and hence rules out the existence of waves in steady coronal structures.

1. Introduction

The study of coronal emission line profiles tells about the physical and dynamical state of coronal structures such as temperature, density, turbulence and mass motions. Coronal emission lines have been observed, one at a time over a large coronal region or multiple on limited coronal region using Fabry–Pérot techniques or spectrographs during total solar eclipses and with coronagraphs at high altitudes (Singh, 1985; Delone and Makarova, 1975; Tsubaki, 1977; Livingston and Harvey 1982; Liebenberg, Bessey, and Watson, 1975; Bessey and Liebenberg, 1984; Raju *et al.*, 1993; Ichimoto *et al.*, 1995; Hara and Ichimoto, 1999, and others). With the advent of space observations, a large data base is now available in the EUV, soft X-ray and hard X-ray spectral regions representing the chromosphere-corona transition region and inner solar corona (Doschek *et al.*, 1976; Athay, Gurman, and Henze, 1983; Domingo, Fleck, and Poland, 1995; Brynildsen *et al.*, 1998; Seely *et al.*, 1997, and others).

Solar Physics **212:** 343–359, 2003.

The ionization temperature associated with an emission line predicts a certain line width for that line. The excess observed line width of the coronal emission lines has been referred as 'nonthermal width' or 'nonthermal velocity' in terms of velocity. Hassler *et al.* (1990) and many other authors have interpreted this nonthermal component as mass motions by hydromagnetic waves. Doschek and Feldman (2000) have determined nonthermal motions as a function of position in streamer regions from the FWHMs of EUV spectral line profiles under the assumption that the ion temperature equals the electron temperature of the streamer plasma, in the range of 20–40 km s^{-1}. Recently, Doschek *et al.* (2001) have determined the nonthermal motions as a function of height above the limb in polar coronal holes from EUV spectral lines. They found that the nonthermal motions sometimes, but not always, increase slightly with the height above the limb.

With the easy availability of low-noise, large-dynamic-range and large-format CCD cameras, it has now become feasible to obtain spectra of coronal emission lines to moderate height above the limb at high dispersion and resolution in the visible portion of the spectrum using a coronagraph. Singh *et al.* (1999, Paper I) obtained spectra in the green and red lines simultaneously on several days covering several coronal regions to study the variation in line profiles as a function of height. They used the line intensity as a proxy of the height above the limb and found that the FWHM of the red (6374 Å [Fe X]) line increases with height and that of the green (5303 Å [Fe XIV]) line decreases with height. Singh *et al.* (2002a, Paper II) computed the gradients of the FWHM of these lines as a function of height from the linear fits to the data of several different coronal structures, but their main interest was on time variability, and the data samples were limited. Singh *et al.* (2002b, Paper III) analyzed the red [Fe X] and infrared [Fe XIII] spectral lines, but their aim was density diagnostics. Paper IV by Singh *et al.* (2002c) deals with thorough statistical study based on a larger sample of data obtained simultaneously in the red and green; and red and infrared coronal emission lines for a comparative study of the gradients of FWHM of these lines.

The spectra of green, infrared and red emission lines represent plasma at about 2.1, 1.6, and 1.0 $\times 10^6$ K, respectively. The coronal emission line at 7892 Å represents plasma at a temperature little more than that of the red line. The coronal structures observed in the red and 7892 Å lines are expected to show more similarity in the appearance of structures and similar behavior in the variation of FWHM with the height. In this paper we discuss the variation of line width of both the red and 7892 Å coronal emission lines. We also discuss the relationship between the FWHM gradients of the green, infrared, red, and 7892 Å emission lines and the ionization temperatures of the ions involved and its implications for the physical state of steady coronal structures and heating of solar corona.

2. Observations

Spectroscopic observations in the red (6374 Å [Fe X]) and 7892 Å [Fe XI] coronal emission lines were obtained simultaneously with the 25-cm coronagraph of Norikura Observatory. The coude-type coronagraph provided us with a coronal image with an image scale of 25″ per mm and the 7-m focal length the Littrow spectrograph permitted us to mount two CCD cameras to record two different portions of the spectrum around these two coronal emission lines. A CCD camera of 512×512 format with a pixel size of 13.5×13.5 micron was directly mounted at the Littrow focus of the main spectrograph to obtain the spectrum around the 7892 Å emission line in the 3rd order. The second CCD camera of 1024×1024 format with a pixel size of 24×24 micron coupled with the 20-cm aperture and 8.86-m focal length of the Cassegrain telescope was kept to receive the diffracted beam from the grating that over-spilled the Littrow mirror of the main spectrograph to record the spectrum around the red line. The binned CCD cameras yielded a dispersion of 47 mÅ per pixel for the 4th-order red line and 48 mÅ per pixel for the 3rd-order 7892 Å emission line. The large slit width of 160 microns, used while making the observations, corresponds to 112 mÅ in the red-line spectra and 115 mÅ in the 7892 Å line spectra.

The inclination of the glass block installed in front of the entrance slit was changed to obtain the successive spectra at different locations in the solar corona to get two-dimensional information. The exposure time for recording the red-line spectrum ranged between 15–25 s and that for the 7892 Å line 30–40 s depending upon the sky conditions. To maintain the simultaneity in the observations of both the lines the exposures for both the CCD cameras were started at the same time and the CCD camera for recording the red-line spectrum waited to begin the next exposure till the exposure for the 7892 Å spectrum could be completed. The raster scans at 50 positions with a step size of 4″ could be completed in 30–40 min depending on the exposure time of the 7892 Å line spectrum which was always greater than that for the red line. In all we obtained 14 raster scans covering three different coronal regions on 20 September 1998; nine raster scans over one coronal region, four raster scans over the second and one scan on the third. The whole set of observations lasted over a period of about 9.5 hours. The details of the observations are listed in Table I.

3. Data Analysis

While recording the spectra, the CCD pixels were binned to give a resolution of about $2'' \times 2''$, but the slit width of 4″ restricted the spatial resolution to $2'' \times 4''$. All the spectra were corrected for the dark current and the sky component due to scattered light using a spectrum of the defocussed solar disc. A Gaussian fit was made to the emission line profile at each location in the observed coronal region

TABLE I

Epoch, location of coronal region, mean values of FWHM gradient (mÅ arc sec^{-1}) and FWHM (mÅ) of the 7892 Å and red line at 50″ and 100″ for the observations made on 19–20 September 1998.

Epoch (UT)		Coronal	FWHM gradient		7892 Å FWHM		6374 Å FWHM	
h	min	region	7892 Å	6374 Å	50″	100″	50″	100″
21	12	N–W	−0.41	0.63	1141	1120	870	901
21	50	N–W	−0.07	0.29	1099	1096	837	851
00	20	N–W	−0.05	0.13	1116	1114	848	855
02	00	N–W	0.01	0.29	1109	1109	833	847
02	46	N–W	−0.06	0.09	1119	1116	845	849
04	34	N–W	0.03	0.19	1104	1106	843	852
06	10	N–W	−0.07	0.07	1092	1088	846	849
07	33	N–W	−0.19	0.20	1082	1072	846	856
08	01	N–W	−1.05	0.46	1108	1056	856	879
22	45	E	−0.23	0.26	1116	1104	854	867
23	28	E	−0.41	0.00	1122	1102	868	867
01	08	E	−0.69	0.14	1120	1085	864	871
07	02	E	0.07	0.55	1086	1090	880	908
03	36	S–W	−0.85	−1.10	1132	1090	871	815
Mean			−0.28	0.16	1110	1096	854	862

discarding data points at the locations of the absorption line coinciding with the emission line to ensure the reliability of the fit; the peak intensity, central wavelength and width of the emission line were computed from each of the Gaussian curve. The 1/e width (w) computed from the Gaussian fit is defined as

$$I(\lambda - \lambda_0) = I(\lambda_0) e^{-\frac{1}{2}(\frac{\lambda-\lambda_0}{\omega})^2}.$$

In the top panel of Figure 1(a) we show a typical observed profile of the red emission line. The bottom panel shows the residual emission profile after the correction and the Gaussian fit to the residual profile plotted over it. Figure 1(b) shows a typical observed profile of the 7892 Å line, the corrected profile and the Gaussian fit. The errors in the parameters provided by standard IDL computer programs for both the emission lines for a coronal structure near the limb and at 100″ above the limb are listed in Table II. The values of the parameters vary depending upon the coronal structure and locations above the limb whereas the values of errors are typical. These values indicate that the errors in the computed values of relative amplitude, central wavelength and FWHM of the emission lines from the Gaussian fits to the data are negligibly small.

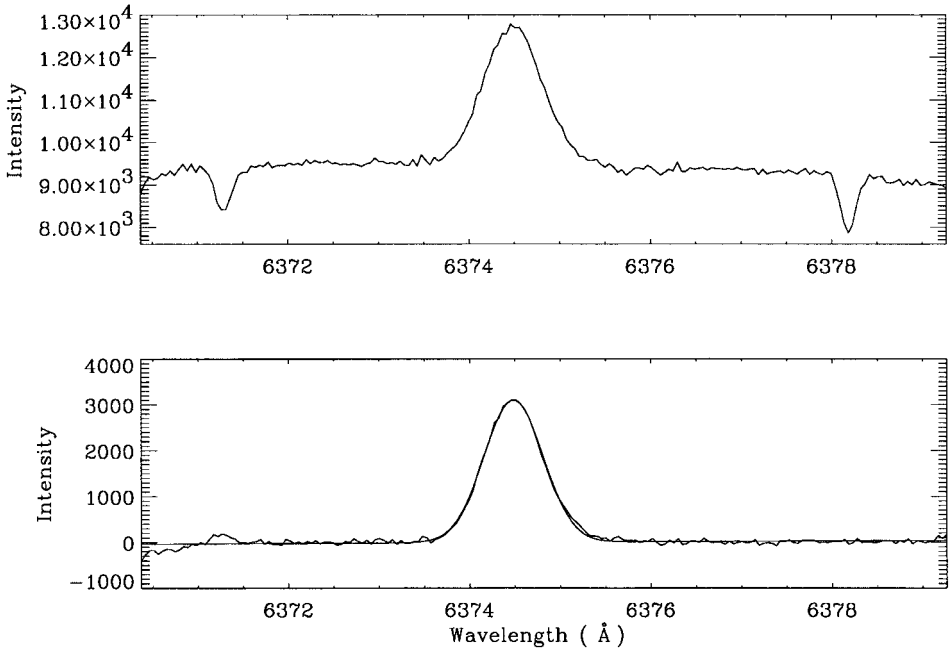

Figure 1a. The *top panel* shows a typical observed profile of the red coronal emission line at 6374 Å. The *bottom panel* shows the residual profile after correction for dark, flat field and photospheric scattered light along with a Gaussian fit to the residual profile.

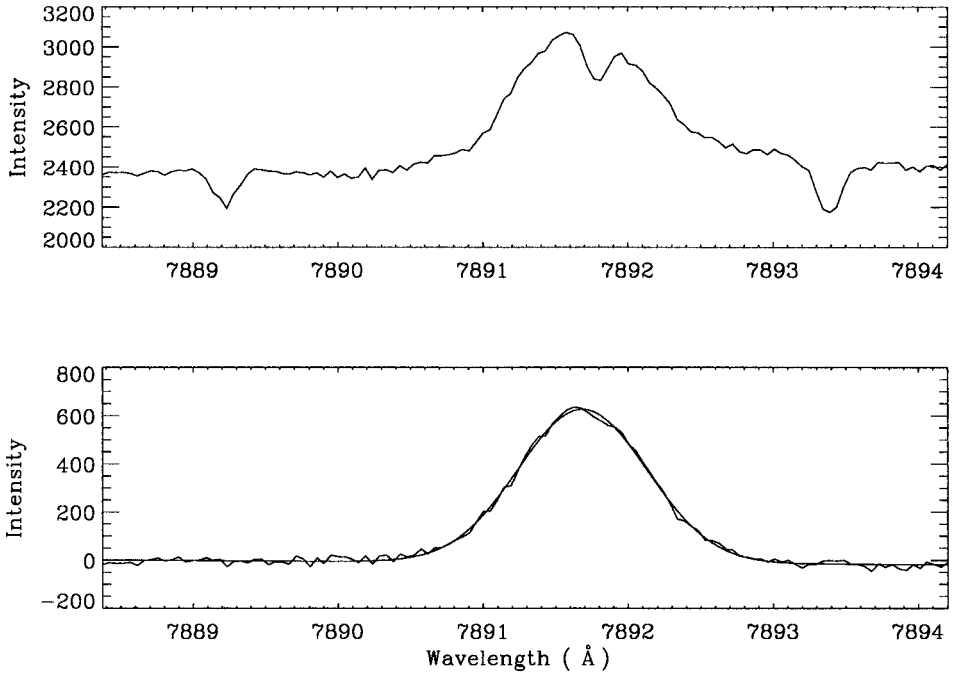

Figure 1b. Same as Figure 1(a), but for the [Fe XI] coronal emission line at 7892 Å.

TABLE II

Parameters of coronal emission lines computed from the Gaussian fit by standard IDL software for a coronal structure. Errors are typical of more parameters derived for other structures.

	Near the limb	At 100″ above the limb
For the red (6374 Å [Fe X]) line:		
Relative amplitude	3432.8 ± 0.34	521.8 ± 0.33
FWHM	0.817 ± 0.001 Å	0.861 ± 0.001 Å
Wavelength	6374.48 ± 0.001 Å	6374.44 ± 0.001 Å
For the 7892 Å [Fe XI] line:		
Relative amplitude	897.2 ± 0.30	189.0 ± 0.31
FWHM	1.117 ± 0.001 Å	1.138 ± 0.002 Å
Wavelength	7891.65 ± 0.001 Å	7891.66 ± 0.001 Å

The derived values were plotted as a function of spatial locations to obtain spectroheliograms, velocitygrams and widthgrams of the observed coronal region. Figure 2 is a typical example of such a plot. The top panels show the intensity distribution, the middle panels show velocity distribution and the bottom panels indicate the line width distribution in the red and 7892 Å emission lines. The top panels of Figures 2 indicate the similarity in the coronal structures as expected. The widthgrams appear to show a small variation with height along the coronal structure.

The image scale of the red and 7892 Å lines spectra is 2.02″ and 2.33″, respectively. The image scales of these spectra and heliograms are different due to different effective focal lengths of the optics used to image. The data were rescaled to make all the heliograms the same spatial scale and dimensions using a solar disk spectrum obtained with three fiducial marks made by three wires in front of the entrance slit of the spectrograph.

To begin with all the coronal structures visible in the observed region were considered together, and the line widths, relative intensities and velocities were computed to see the general trend in these parameters as a function of height. We selected 200–300 locations with a resolution of $4'' \times 4''$ on various coronal structures visible in the red line images, shown by + in Figure 3(a). The corresponding locations in other images were selected automatically using software to generate Figure 4. The FWHM of the emission lines were computed using the relation

$$\mathrm{FWHM} = w(2(2\ln 2)^{1/2})$$

and it was corrected for the instrumental effects using the standard equation

$$\mathrm{FWHM}_{\mathrm{corr}} = (\mathrm{FWHM}^2_{\mathrm{obs}} - \mathrm{FWHM}^2_{\mathrm{instrument}})^{1/2}.$$

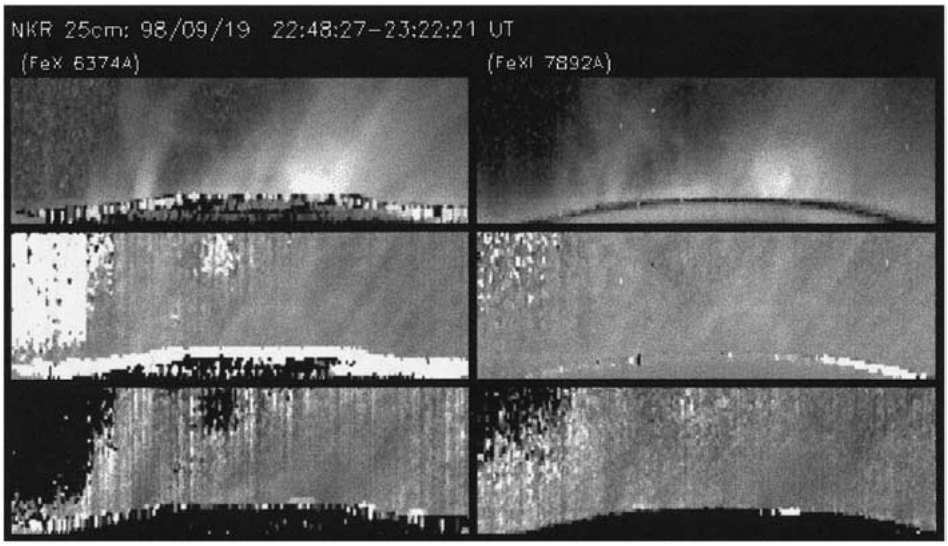

Figure 2. The images of the solar corona constructed from the red and 7892 Å emission lines. The *top row* shows distribution of the red and 7892 Å line intensities. The *middle* and *bottom rows* indicate the velocity and line-width distributions, respectively.

The top panel of Figure 4 shows the red-line intensity versus 7892 Å line intensity, the middle panel the FWHM of the red ($*$) and 7892 Å(Δ) lines as a function of height above the limb along with the linear fits to the respective data sets, and the bottom panel the intensity ratio ($I_{7892}/I_{\rm red}$) against height in arc sec. Similarly we have done the analysis of individual coronal structures by selecting 10–20 locations depending upon the extent of the structure as shown in Figure 3(b) by a + sign. Figure 5 shows intensities, intensity ratio and FWHM of these two emission lines as in Figure 4, but for an individual coronal structure. We have derived the gradient of FWHM, and FWHM at $50''$ and $100''$ of both of the red and 7892 Å emission lines from the linear fits to the respective data sets of FWHM as a function of height for the coronal region as a whole as well as for individual coronal structures.

4. Results

Figure 4, which is for the entire coronal region, shows that the FWHM of the red line increases with height whereas that for the 7892 Å emission line decreases with height above the limb. Figure 5, that is for an individual structure, shows that the line width of both the red and 7892 Å lines increases with height and shows that the scatter in the data for individual structure, is much less as compared to the scatter in the entire coronal region data. This implies that different individual structures are in different physical states. In most of the individual coronal structures the FWHM

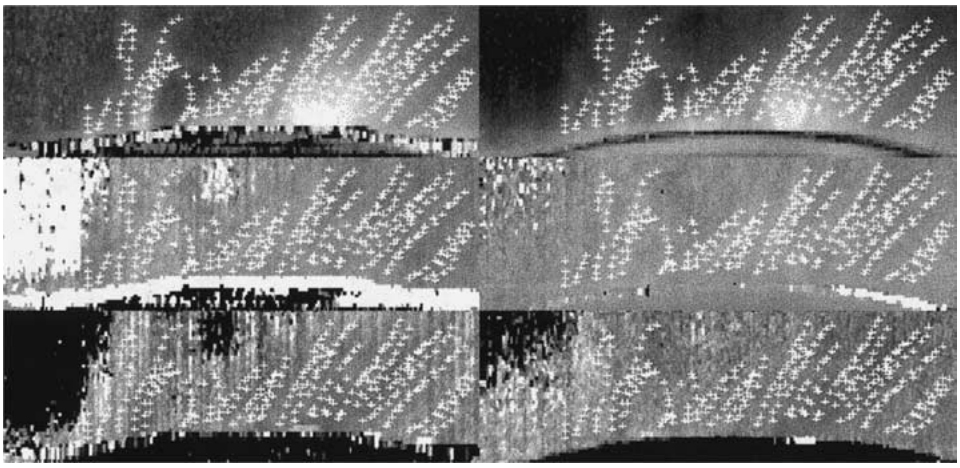

Figure 3a. Same as Figure 2. The + sign indicates the locations on coronal structures where the values of line width, intensity and velocity have been determined to generate Figure 4.

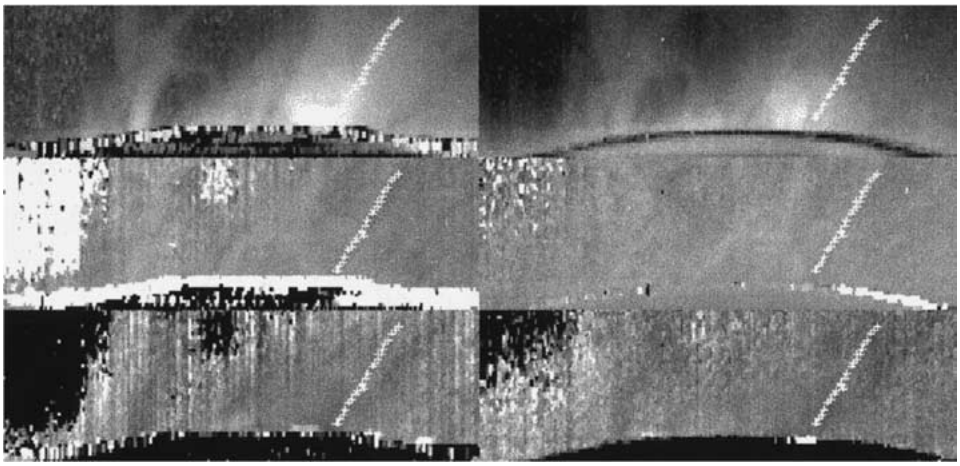

Figure 3b. Same as for Figure 3(a) but for an individual coronal structure. The + sign indicates locations along an individual structure used to generate Figure 5.

of both the emission lines increases with height. It is not clear why the FWHM of the 7892 Å line decreases with height when all the structures were considered together while in most of individual coronal structures it increases with height. We list in Table I the epoch of observations, location of coronal region, mean gradient of FWHM of both the lines in mÅ arc sec^{-1}, and mean FWHM (mÅ) at $50''$ and $100''$ for the coronal region. These values indicate that for most of the coronal regions, the FWHM of the 7892 Å line decreases with height whereas that of the red line increases with height above the limb. The mean value of FWHM gradient for the red line is small as compared to that for other coronal regions observed with green and infrared lines (Singh *et al.*, 2002c). The reason for this may be that large

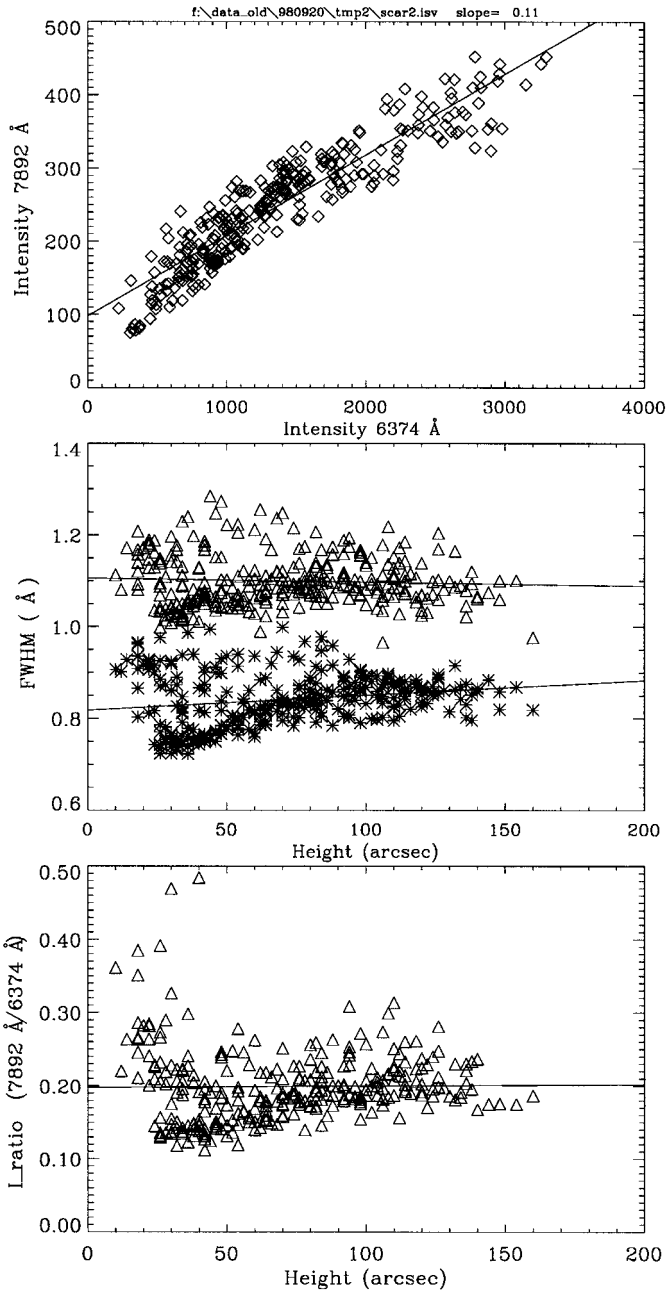

Figure 4. A typical plot made after computing the values of line width, intensity and velocity over $4'' \times 4''$ considering all the structures together in a coronal region. The *top panel* shows the variation of 7892 Å [Fe XI] line intensity versus the red-line intensity. The *middle panel* represents the FWHM of the 7892 Å(Δ) and red line ($*$) as a function of height above the limb along with the linear fits (*straight lines*) to the respective data sets. The *bottom panel* indicates the intensity ratio ($I_{7892}/I_{\rm red}$) versus height above the solar limb.

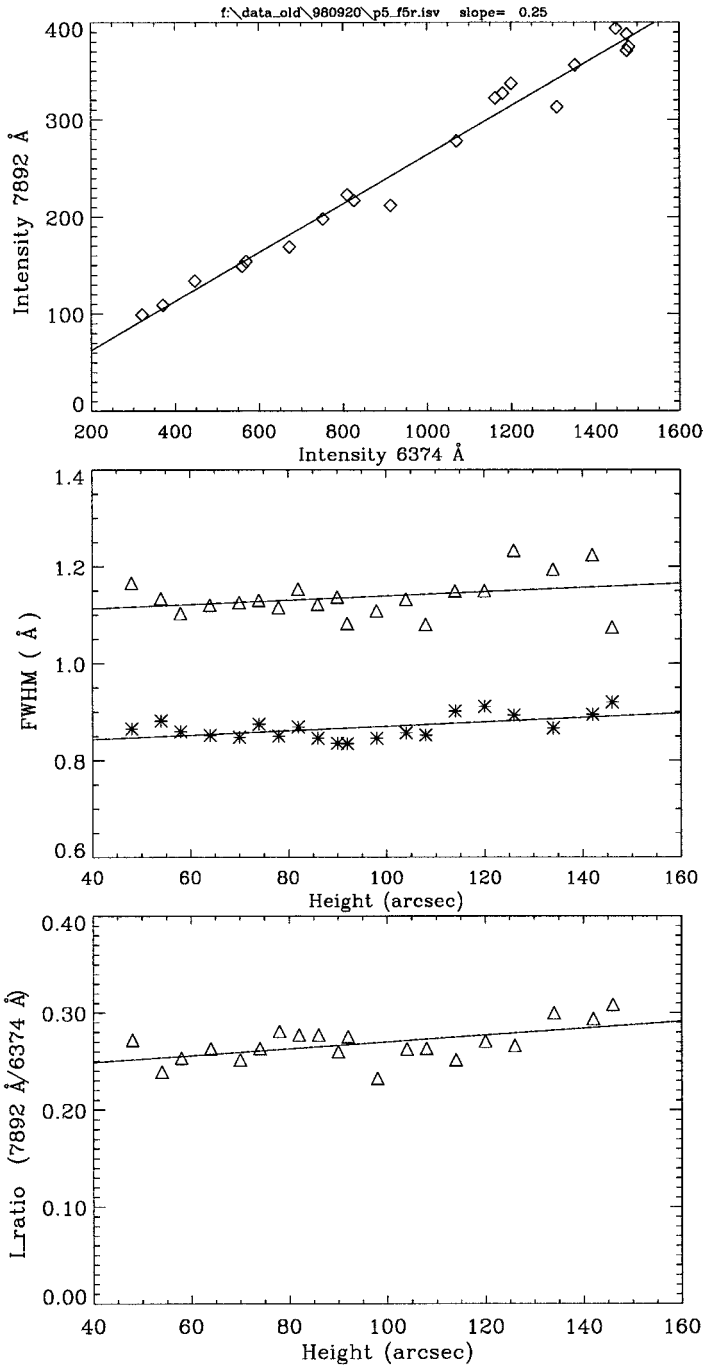

Figure 5. Same as Figure 4, but for an individual coronal structure.

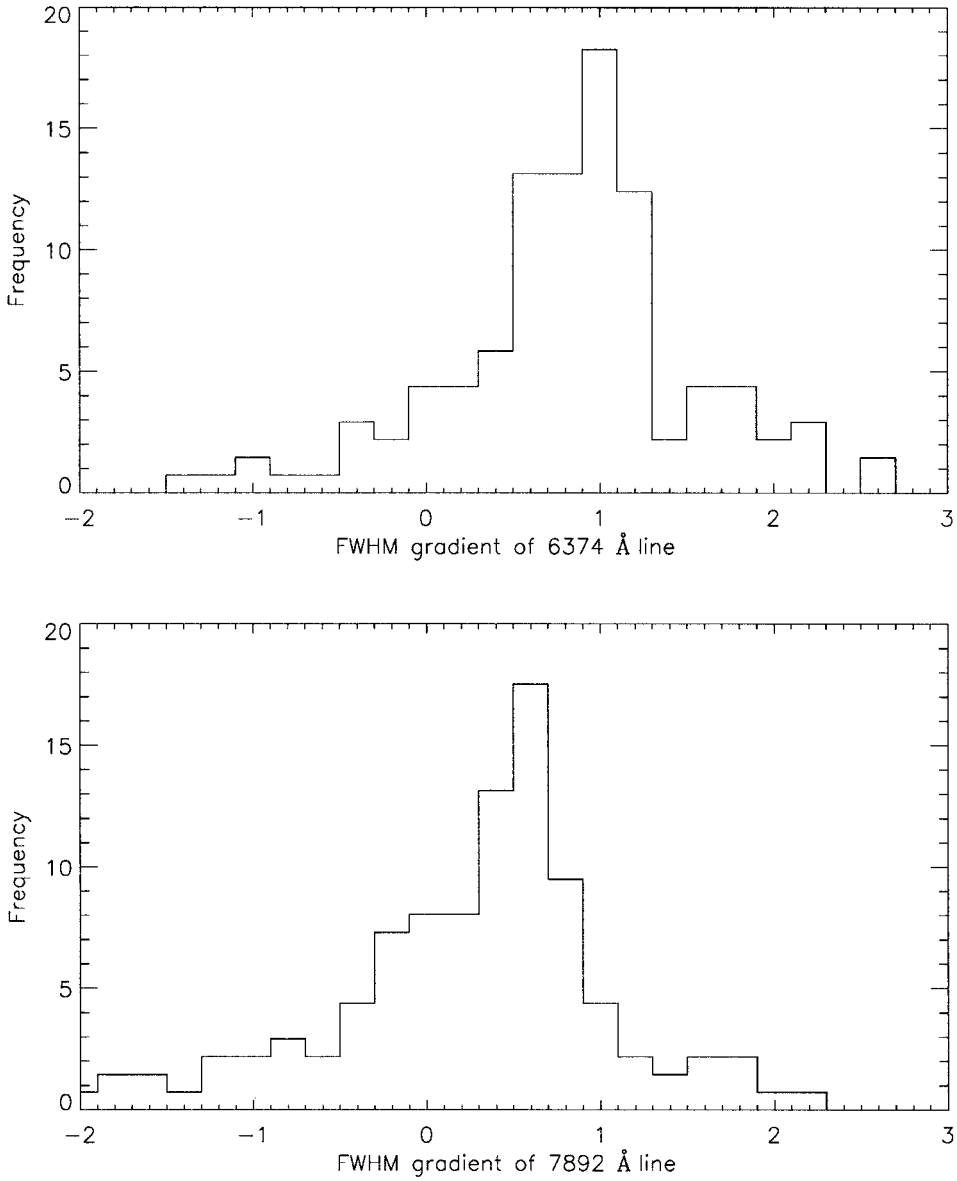

Figure 6. The *top panel* shows the frequency distribution of FWHM gradient for the red line. The *bottom panel* indicates the same for the 7892 Å [Fe XI] line.

differences in the physical properties of the individual coronal structures yield a small mean value.

We have analysed 136 individual coronal structures to determine the variations in the line parameters as a function of height above the limb. To compare the FWHM gradients for different coronal emission lines we have plotted the fre-

quency distribution for both the red and 7892 Å lines in Figure 6. The figure shows that 89% of the individual structures have positive gradient with a most probable value of 0.95 mÅ arc sec^{-1} when observed in the red line whereas 71% have a positive gradient with a most probable value of 0.55 mÅ arc sec^{-1} when observed in the 7892 Å line. The above most probable value of FWHM gradient for the red line agrees with that found earlier by Singh *et al.* (2002c) from their simultaneous observations of the red and green, and red and infrared lines. It is not clear why for the red line the most probable value of gradient of FWHM is much larger than the mean value derived considering all the individual structures in the coronal regions and for the 7892 Å line the most probable value is positive while the mean value is negative. More data are needed to understand such a behaviour. In general, we may say that FWHM of both the red and 7892 Å line increases with height above the limb and FWHM of the red line increases faster than that for the 7892 Å line. To determine the most probable values of FWHM at two different heights and then compute nonthermal velocity we have plotted the frequency distribution of FWHM for these emission lines in Figure 7. The figure indicates that at 50″ and 100″ the most probable values of FWHM of the red line are 820 mÅ and 850 mÅ, respectively and those for the 7892 Å line are 1095 mÅ and 1110 mÅ. These values confirm that FWHM of these lines increases with height above the limb.

A plot of the FWHM gradients of the red line against those for the 7892 Å line shown in the top panel of Figure 8 and the linear fit to the data indicate that FWHM gradients of the red and 7892 Å lines are correlated. A correlation coefficient of 0.56 implies a confidence level of about 97%. The plots between the FWHM gradients and the gradients of intensity ratio of 7892 Å/red lines show that the red-line FWHM gradient is better correlated with the intensity-ratio gradient than that for the 7892 Å line (the middle and bottom panel of Figure 8). From these results we may say that generally the variations in the parameters of both the red and 7892 Å lines are correlated, but we need to confirm these results using more simultaneous data.

5. Discussion

We list the mean values of the FWHM at 50″ and 100″, and the gradients of FWHM for both the red and 7892 Å coronal emission lines in Table III. For a comparison we also give these values for the infrared and green lines from our earlier paper (Singh *et al.*, 2002c) and temperatures at which the abundances of the ions are maximum (Allen, 1973). Simultaneous observations in two coronal emission lines have been made choosing a combination of either the red and green or the red and infrared, or the red and 7892 Å lines. Thus the red line has always been observed while making observations in the green or the infrared or the 7892 Å emission lines. The values for the red line given in Table III are averages over all these observations. We find that the line widths of both the red and 7892 Å lines increase

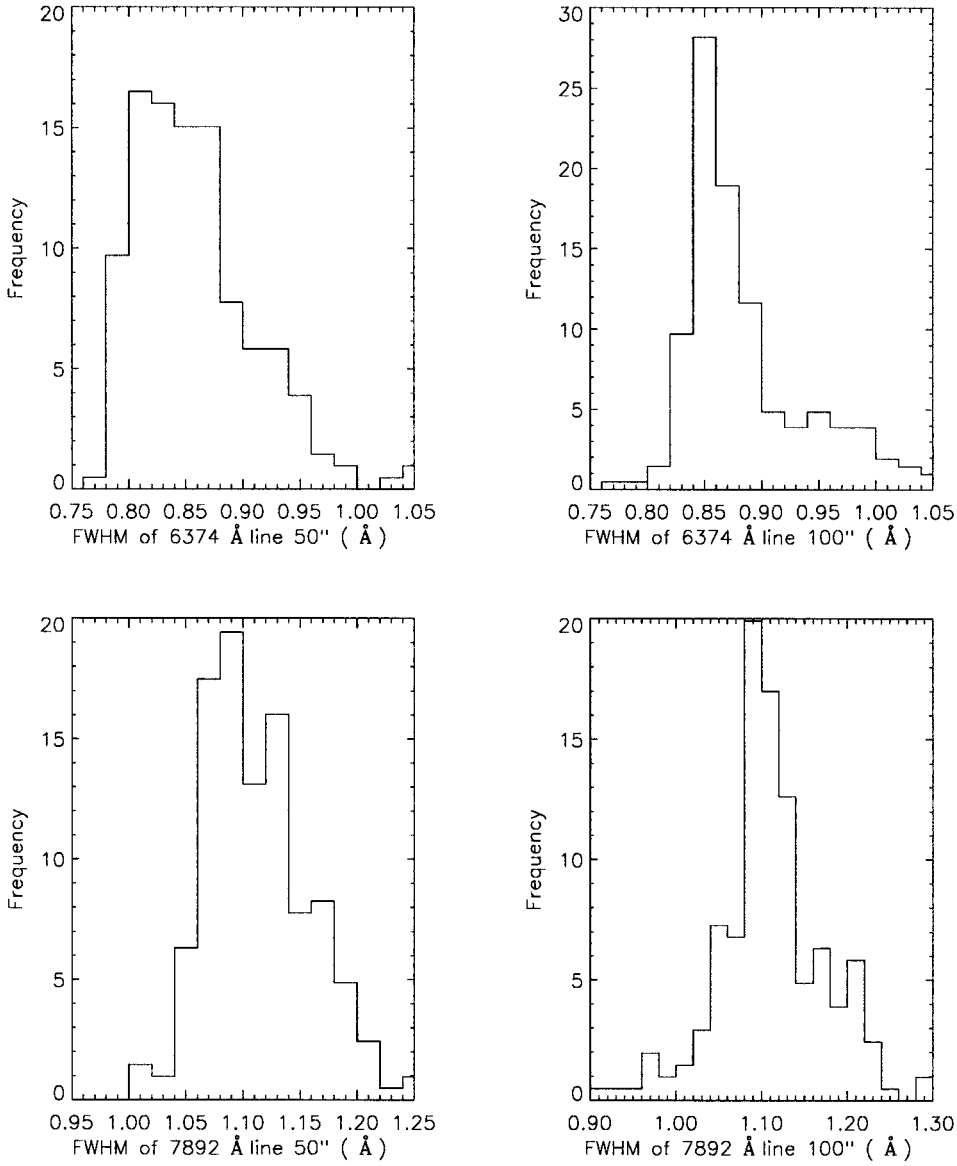

Figure 7. The frequency distribution of FWHM of the red and 7892 Å [Fe XI] coronal emission lines at 50″ and 100″ derived from the linear fits to data of individual coronal structures.

with height for most of the individual coronal structures. The increase in FWHM of the red line is larger than that for the 7892 Å. The most probable values of FWHM gradient for the red and 7892 Å lines are 0.95 and 0.55 mÅ arc sec^{-1}, respectively.

Assuming the kinetic temperature to be the same as the ionization temperature (one million) for the Fe IX ion, we compute the average values of nonthermal velocities as 16.6 km s^{-1} and 18.7 km s^{-1} at 50″ and 100″, respectively. Similarly we

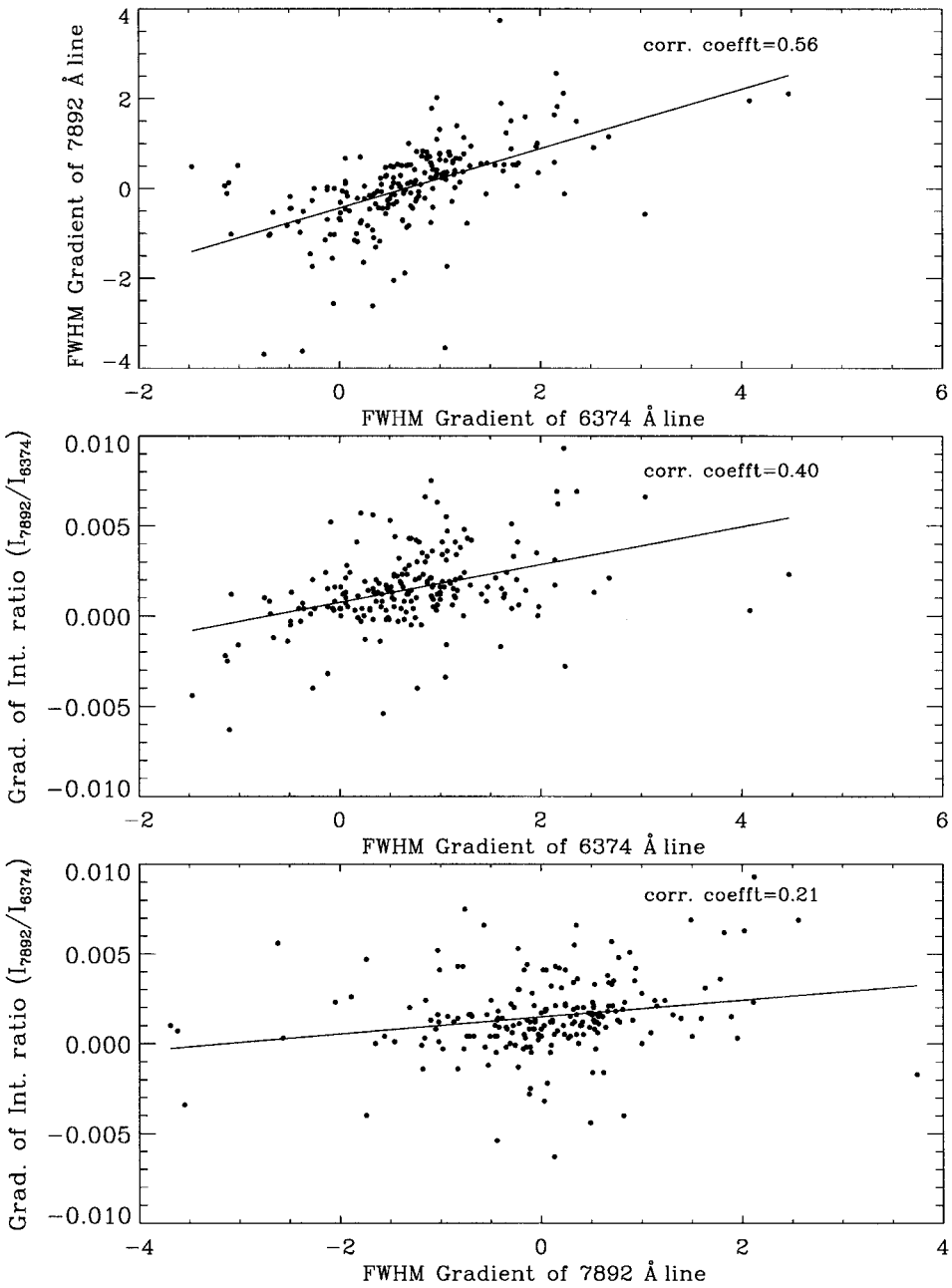

Figure 8. The *top panel* shows FWHM gradient of the red (6374 Å [Fe X]) line against that of 7892 Å [Fe XI] line. The *middle* and *bottom panels* show the relationship between the FWHM gradients and intensity ratio ($I_{7892}/I_{\rm red}$).

TABLE III
Mean value of FWHM (Å) and its gradient (mÅ arc sec^{-1}) of coronal emission lines.

Emission line	FWHM (50″)	FWHM (100″)	FWHM gradient	FWHM gradient/λ	Ionization temp.(MK)
Red [Fe X]	0.846 ± 0.052	0.898 ± 0.064	1.05	1.65×10^{-4}	1.00
7892 Å [Fe XI]	1.098 ± 0.087	1.126 ± 0.098	0.57	0.72×10^{-4}	1.29
Infrared [Fe XIII]	1.890 ± 0.103	1.905 ± 0.126	0.29	0.26×10^{-4}	1.62
Green [Fe XIV]	0.822 ± 0.049	0.789 ± 0.063	−0.66	-1.25×10^{-4}	2.09

find an average value of 15.6 km s^{-1} from the 7892 Å line observations at 50″ by taking $T = 1.3 \times 10^6$ K. If we consider that the nonthermal velocity increases by 2.1 km s^{-1} at 100″ from its value at 50″ as computed for the red line, the FWHM of the 7892 Å line should be larger by 60 mÅ at 100″ when compared to that at 50″, but we find that it is larger by 28 mÅ only. From the observed values of the FWHM gradients of these two lines and those of the green and infrared lines (Singh *et al.*, 2002c) we can say that the FWHM of all these lines do not increase by the same amount with height above the limb. The plot shown in Figure 9 indicates that the FWHM gradient normalised with respect to its wavelength is inversely related to the ionization temperature associated with the emission line and the variation is almost linear. As the ionization temperature increases the value of the FWHM gradient decreases and becomes negative for relatively high temperature lines. The linear fit to the data in Figure 9 indicates that the FWHM gradient is positive for emission lines representing an ionization temperature less than 1.7×10^6 K and negative for others. The observations in the red and 7892 Å coronal emission lines agree well with the scenario speculated by Singh *et al.* (2002c) from the results of earlier observations in the red, infrared, and green emission lines.

If the nonthermal velocity or temperature or both increase with height in steady coronal structures, all these emission lines must show an increase in the FWHM with height and the increase is expected to be proportional to the wavelength of the line. But the observed variations of FWHM in different emission lines as a function of height do not agree with this scenario. Doyle, Banerjee, and Perez (1998) have observed the increase in the FWHM of Si VIII line above the limb and interpreted it as due to undamped radially propagating Alfvén waves. But our results from the simultaneous observations of two coronal emission lines (selecting 2 at a time out of the 4 coronal emission lines) rules out the existence of waves in the steady coronal structures, since the presence of waves is expected to increase the FWHM of these emission lines proportional to their wavelength. The observed variation in the FWHM of these lines with height can be explained in terms of mixing of plasma

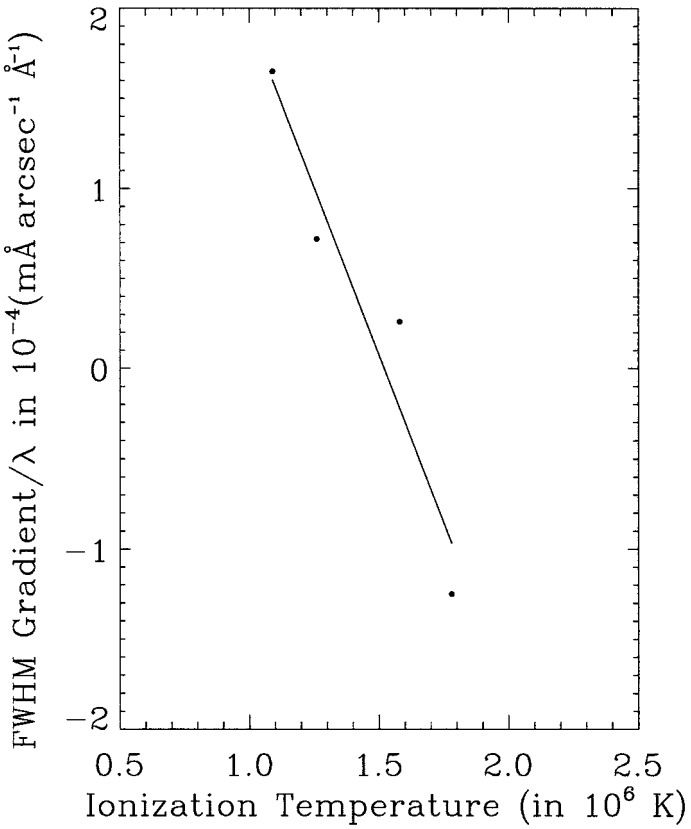

Figure 9. A plot of FWHM gradient/λ for the red, 7892 Å, infrared and green coronal emission lines against the ionization temperature associated with these lines along with a linear fit to the data.

at larger heights as was done earlier for the red- and green-line observations (Singh *et al.*, 1999).

6. Conclusions

We conclude that the variations of the FWHM of the coronal emission lines with height are inversely related with the ionization temperature associated with the emission lines. The values of the FWHM gradient decrease as the ionization temperature increases and finally it becomes negative for relatively high-temperature lines. The values of gradient of the FWHM for different lines varies almost linearly with the ionization temperature associated with the emission lines. This kind of behaviour in the variation of the FWHM gradient suggests that it may not always be possible to interpret an increase in the FWHM of emission line with height as an

increase in nonthermal velocity and thus rules out the existence of waves in steady coronal structures.

Acknowledgements

Jagdev Singh thanks the Director, National Astronomical Observatory of Japan for providing him with the opportunity to work at NAOJ. He also thanks Ramanath Cowsik, Director, Indian Institute of Astrophysics for his encouragement, and A. V. Raveendran, N. K. Pramila and J. S. Nathan for their help.

References

Allen, C. W.: 1973, *Astrophysical Quantities*, The Athlone Press, London, p. 179.
Athay, R. G., Gurman, J. B., and Henze W.: 1983, *Astrophys. J.* **269**, 706.
Bessey, R. J. and Liebenberg, D. H.: 1984, *Solar Phys.* **94**, 239.
Brynildsen, N., Brekke, P., Fredvik, T., Haugan, S.V.H., Kjeldseth-Moe, O., Maltby, P., Harrison, R. A., and Wilhelm, K.: 1998, *Solar Phys.* **181**, 23.
Delone, A. B. and Makarova, E. A.: 1975, *Solar Phys.* **45**, 157.
Domingo, V., Fleck, B., and Poland, A. I.: 1995, *Solar Phys.* **162**, 1.
Doschek, G. A. and Feldman, U.: 2000, *Astrophys. J.* **529**, 599.
Doschek, G. A., Feldman, U., VanHoosier, M. E., and Bartoe, J. D. F.: 1976, *Astrophys. Suppl.* **31**, 417.
Doschek, G. A., Feldman, U., Laming, J. M., Schuhle, U., and Wilhelm, K.: 2001, *Astrophys. J.* **546**, 559.
Doyle, J. G., Banerjee, D., and Perez, M. E.: 1998, *Solar Phys.* **181**, 91.
Hara, H. and Ichimoto, K.: 1999, *Astrophys. J.* **513**, 969.
Hassler, D. M., Rottman, G. J., Shoub, E. C., and Holzer, T. E.: 1990, *Astrophys. J.* **348**, L77.
Ichimoto, K., Hara, H., Takeda, A., Kumagai, K., Sakurai, T., Shimizu, T., and Hudson, H. S.: 1995, *Astrophys. J.* **445**, 978.
Liebenberg, D. H., Bessey, R. J., and Watson, B.: 1975, *Solar Phys.* **44**, 345.
Livingston, W. and Harvey, J.: 1982, *Proc. of INSA*, Indian National Science Academy, New Delhi, 48A, 18.
Raju, K. P., Desai, J. N., Chandrasekhar, T., and Ashok, N. M.: 1993, *Monthly Notices Royal Astron. Soc.* **263**, 789.
Seely, J. F., Feldman, U., Schuhle, U., Wilhelm, K., Curdt, W., and Lemaire, P.: 1997, *Astrophys. J.* **484**, L87.
Singh, J.: 1985, *Solar Phys.* **95**, 253.
Singh, J., Ichimoto, K., Imai, H., Sakurai, T., and Takeda, A.: 1999, *Publ. Astron. Soc. Japan* **51**, 269 (Paper I).
Singh, J., Sakurai, T., Ichimoto, K., Suematsu, Y., and Takeda, A.: 2002a, *Publ. Astron. Soc. Japan* **54**, 793 (Paper II).
Singh, J., Sakurai,T., Ichimoto, K., and Takeda, A.: 2002b, *Publ. Astron. Soc. Japan* **54**, 807 (Paper III).
Singh, J., Ichimoto, K., Sakurai, T., and Muneer, S.: 2002c, *Astrophys. J.*, accepted (Paper IV).
Tsubaki, T.: 1977, *Solar Phys.* **51**, 121.